THE ASTROPHYSICAL JOURNAL, 577:853–865, 2002 October 1
© 2002. The American Astronomical Society. All rights reserved. Printed in U.S.A.

THE *r*-PROCESS IN THE NEUTRINO WINDS OF CORE-COLLAPSE SUPERNOVAE AND U-Th COSMOCHRONOLOGY

SHINYA WANAJO AND NAOKI ITOH
Department of Physics, Sophia University, 7-1 Kioi-cho, Chiyoda-ku, Tokyo 102-8554, Japan;
wanajo@sophia.ac.jp, n_itoh@sophia.ac.jp

YUHRI ISHIMARU
Institut d'Astrophysique de Paris, 98 bis Boulevard Arago, F-75014 Paris, France; ishimaru@iap.fr

SATOSHI NOZAWA
Josai Junior College for Women, 1-1 Keyakidai, Sakado-shi, Saitama 350-0290, Japan; snozawa@venus.josai.ac.jp

AND

TIMOTHY C. BEERS
Department of Physics and Astronomy, Michigan State University, East Lansing, MI 48824; beers@pa.msu.edu
Received 2002 February 20; accepted 2002 June 8

ABSTRACT

The discovery of the second highly *r*-process–enhanced, extremely metal poor star, CS 31082-001 ([Fe/H] = −2.9) has provided a powerful new tool for age determination by virtue of the detection and measurement of the radioactive species uranium and thorium. Because the half-life of ^{238}U is one-third that of ^{232}Th, the U-Th pair can, in principle, provide a far more precise cosmochronometer than the Th-Eu pair that has been used in previous investigations. In the application of this chronometer, the age of (the progenitor of) CS 31082-001 can be regarded as the minimum age of the Galaxy, and hence of the universe. One of the serious limitations of this approach, however, is that predictions of the production ratio of U and Th have not been made in the context of a realistic astrophysical model of the *r*-process. We have endeavored to produce such a model, based on the "neutrino winds" that are expected to arise from the nascent neutron star of a core-collapse supernova. In this model, the proto–neutron star mass and the (asymptotic) neutrino sphere radius are assumed to be 2.0 $M_\odot$ and 10 km, respectively. Recent hydrodynamic studies indicate that there may exist difficulties in obtaining such a compact (massive and/or small in radius) remnant. Nevertheless, we utilize this set of parameter choices since previous work suggests that the third *r*-process peak (and thus U and Th) is hardly reached when one adopts a less compact proto–neutron star in the framework of the neutrino-wind scenario. The temperature and density histories of the material involved in the neutron-capture processes are obtained with the assumption of a steady flow of the neutrino-powered winds, with general relativistic effects taken into account. The electron fraction is taken to be a free parameter, constant with time. The *r*-process nucleosynthesis in these trajectories is calculated with a nuclear reaction network code including actinides up to $Z = 100$. The mass-integrated *r*-process yields, obtained by assuming a simple time evolution of the neutrino luminosity, are compared to the available spectroscopic elemental abundance data of CS 31082-001. As a result, the "age" of this star is determined to be 14.1 ± 2.5 Gyr, in excellent agreement with lower limits on the age of the universe estimated by other dating techniques, as well as with other stellar radioactive age estimates. Future measurements of Pt and Pb in this star, as well as expansion of searches for additional *r*-process–enhanced, metal-poor stars (especially those in which both U and Th are measurable), are of special importance to constrain the current astrophysical models for the *r*-process.

Subject headings: nuclear reactions, nucleosynthesis, abundances — stars: abundances — supernovae: general

On-line material: color figures

1. INTRODUCTION

Uranium and thorium are regarded as potentially useful cosmochronometers because their long radioactive decay half-lives (^{232}Th: 14.05 Gyr; ^{238}U: 4.468 Gyr) are significant fractions of the expected age of the universe. All of the actinides, including uranium and thorium, are thought to be pure *r*-process elements, since the alternative neutron-capture process, the *s*-process, terminates at ^{209}Bi. The excellent agreement of the relative abundances of neutron-capture elements in the extremely metal poor ([Fe/H] = −3.1), *r*-process element–enhanced star CS 22892-052 with the solar *r*-process pattern initially suggested that thorium might serve as a precise cosmochronometer (Sneden et al. 1996). The time that has passed since the production of the thorium that is now observed in the outer atmosphere of such an old halo star can be regarded as a hard lower limit on the age of the universe.[1] Sneden et al. (1996) estimated the age of this star to be

[1] For convenience of nomenclature, in the context of radioactive cosmochronology it is common practice to refer to the "age" of a given star as the time difference between the production event (or events) of the radioactive (and stable *r*-process) species that have been incorporated into the outer atmosphere of a low-mass (<0.8 $M_\odot$) star that has not yet evolved past the giant branch stage of evolution and hence is amenable to spectroscopic study.

15.2 ± 3.7 Gyr, comparing the measured Th/Eu ratio with an initial production ratio constrained by theory. This age limit, albeit with a rather large error bar, is in good agreement with the age limits derived by completely different techniques, e.g., for globular clusters (12.9 ± 2.9 Gyr; Carretta et al. 2000), for Type Ia supernovae (14.9 ± 1.4 Gyr; Perlmutter et al. 1999), and from the shape of acoustic peaks in the cosmic microwave background spectrum (14.0 ± 0.5 Gyr; Knox, Christensen, & Skordis 2001).

One advantage of the thorium chronology is that, once the initial and current values of Th/r in the star are specified, the age of the star depends only on the half-life of ^{232}Th determined in the laboratory. That is, one is not forced to invoke complex (and no doubt incomplete) models of Galactic chemical evolution, although insight from making simple attempts can still be obtained (e.g., Cowan et al. 1997). Here, r denotes one of the stable r-process elements, often taken to be Eu. In the most simple model, the initial value of Th/r may be regarded as that arising from a single supernova that exploded in the near vicinity (and perhaps may have even triggered the formation of) the presently observed star, e.g., CS 22892-052, early in the history of the Galaxy. In fact, the large dispersion of Eu/Fe observed in halo stars (more than 2 orders of magnitude) has been naturally explained by chemical evolution models that make such assumptions (Ishimaru & Wanajo 1999; Tsujimoto, Shigeyama, & Yoshii 2000).

Thus far, the initial production of Th/r has been determined by fitting theoretical nucleosynthesis results to the solar r-process pattern, with the assumption that the r-pattern was *universal* in all astrophysical environments (Cowan et al. 1999; Goriely & Clerbaux 1999). However, a recent abundance analysis of CS 22892-052 with Keck I (HIRES) has shown that the lighter neutron-capture elements ($Z \leq 48$) are distinctly underabundant with respect to the solar pattern, which is well fitted by species with $Z \geq 56$ (Sneden et al. 2000). This implies that there likely exists at least two r-process sites that must be invoked to account for the entire set of elements associated with the r-process (Ishimaru & Wanajo 2000; Qian 2000). Furthermore, it should be noted that although Johnson & Bolte (2001) have derived an estimate of the minimum age of the universe, 11.0 ± 4.2 Gyr, based on the abundances of thorium and other stable neutron-capture elements in five metal-poor stars, the estimated ages of these stars are very widely spread, from $\approx$6 to 18 Gyr (with overlapping error bars). In addition, recent spectroscopic studies of several extremely metal poor halo stars with the Subaru Telescope High-Dispersion Spectrograph has revealed that the spread of estimated chronometric ages from the Th-Eu pair appears to exceed the abundance uncertainties (S. Honda et al. 2002, in preparation). Taken at face value, these results imply that the universality of the r-pattern may not hold over the actinides either.

The second discovered r-process–enhanced, extremely metal poor star, CS 31082-001 ([Fe/H] $= -2.9$) has provided a new, potentially quite powerful cosmochronometer, uranium (Cayrel et al. 2001; Hill et al. 2002). In principle, uranium might be expected to be a more precise chronometer than thorium owing to its shorter half-life. Cayrel et al. (2001) concluded that the age of this star is 12.5 ± 3 Gyr, based on comparisons of the observed ratios of U/Th, U/Os, and U/Ir with their estimated production ratios (Cowan et al. 1999; Goriely & Clerbaux 1999). The discovery of uranium in CS 31082-001 has also prompted additional laboratory work to refine the oscillator strengths, for both uranium and thorium (Nilsson et al. 2002a, 2002b) that are required to turn spectroscopic observations into measured abundances. However, analysis of this star has also provided conclusive evidence that the r-process pattern is *not universal* over the actinides; the ratio Th/Eu in this star is *higher* than that of the solar r-process ratio. CS 31082-001 would be younger than the solar system if the initial Th/Eu were taken to be universal, in conflict with the ages derived from ratios involving U and other stable r-process elements close to the third r-process peak. Therefore, any age estimates that demand assumption of the universality of the r-process pattern may in fact be unreliable.

In addition to the above nonuniversality problem, the initial r-process pattern has thus far been determined theoretically by the superposition of nucleosynthesis results, where one is forced to assume constant temperatures, neutron number densities, and exposure times (or the number of captured neutrons)—the most recent exploration of this approach is presented in Schatz et al. (2002). These approximations have been necessary because of the lack of a reliable astrophysical model for the r-process site (at least that associated with the heavy r-process elements). At the moment, the neutrino-wind scenario is considered to be the most promising, ever since the work by Woosley et al. (1994), although alternative models involving neutron-star mergers have also shown some promise (Freiburghaus, Rosswog, & Thielemann 1999b). However, even the neutrino-wind model encounters serious problems, e.g., the high entropy ($\sim 400 N_A k$) that led to the robust r-processing in the Woosley et al. scenario has not been duplicated by other work (Takahashi, Witti, & Janka 1994; Qian & Woosley 1996).

The purpose of this paper is, therefore, to construct a realistic r-process model based on the neutrino-wind scenario, in order to derive initial production ratios that might be useful for estimation of the minimum age of the universe, in particular by use of the U-Th chronometer pair. Recently, Wanajo et al. (2001) have demonstrated that the solar r-process pattern for $A \approx 120$–200 is well reproduced in such a model from a compact proto–neutron star, owing to the inclusion of general relativistic effects. Although recent hydrodynamic studies have encountered difficulties attaining the required compactness, we use their model along with some improvements to be discussed in § 2. Although some severe problems yet remain, it is clearly important to determine the initial r-process pattern based on site-specific, rather than only site-independent, models. In § 3 the r-process nucleosynthesis calculation is described and the results are compared to the solar r-process pattern. The initial electron fraction, Y_e, is varied from 0.39 to 0.49 but as taken constant with time during the neutron-capture process. In § 4 the age of CS 31082-001 is derived by comparison of the nucleosynthesis results obtained for each Y_e with the abundance pattern of heavy elements in this star. The implications of this study are discussed in § 5.

2. NEUTRINO WINDS

Neutrino winds, in which the free nucleons accelerated by the intense neutrino flux near the neutrino sphere of a core-collapse supernovae assemble to heavier nuclei, have been believed to be the most promising astrophysical site of the r-process since the work by Woosley et al. (1994). The rather

high entropy ($\sim 400 N_A k$) of the ejected matter in their hydrodynamic simulations led to production of the *r*-process elements that is in remarkable agreement with the solar *r*-process pattern. However, subsequent analysis of both hydrodynamic and analytic approaches suggests that such high entropy may not be achieved in neutrino winds ($\sim 100 N_A k$; Takahashi et al. 1994; Qian & Woosley 1996). In addition, an unacceptable overproduction of the elements with $A \approx 90$ appeared in the *r*-process yields of Woosley et al. (1994).

Recently, Otsuki et al. (2000) have studied the physical conditions required for the *r*-process in detail, using a semi-analytic model of a spherical, steady neutrino wind and taking general relativistic effects into account (see also Qian & Woosley 1996; Cardall & Fuller 1997; Thompson, Burrows, & Meyer 2001). They suggested that robust physical conditions for the *r*-process were obtained only if the proto–neutron star was as massive as $\sim 2.0\ M_\odot$. Furthermore, Wanajo et al. (2001) showed from nucleosynthesis calculations that the *r*-process yields for the compact proto–neutron star models (with a mass of 1.9–2.0 $M_\odot$ and radius of 10 km) were in good agreement with the solar *r*-process pattern. This agreement was achieved owing to the short dynamical timescale ($\lesssim 10$ ms) and moderately high entropy ($\gtrsim 140\ N_A k$) obtained at the early phase of the neutrino wind, which prevents most of the free nucleons to assemble into heavy nuclei. There are, however, some severe problems in their models. For example, it would appear difficult to obtain such a compact proto–neutron star with hydrodynamic models of core-collapse supernovae using the equations of state of high-density matter that are currently available. This model also suffered from significant overproduction of elements with $A \approx 90$. Hence, although problems remain, we have chosen to begin with these models, and attempt to refine them in order to see whether progress can be made toward the goal of obtaining more realistic production ratios of heavy elements that might prove useful for the U and Th chronologies.

In this paper we use a model with a proto–neutron star with (gravitational) mass of 2.0 $M_\odot$ and radius of 10 km, as in Wanajo et al. (2001), whose nucleosynthesis results are in good agreement with the solar *r*-pattern for nuclei $A \approx 120$–200. We briefly describe the models here and point out some improvements that have been added.

The system is treated as time stationary and spherically symmetric, and the radius of the neutron star is assumed to be the same as that of the neutrino sphere. The physical variables in the neutrino wind are then functions of the radius only. The mass ejected by neutrino heating is assumed to be negligible compared to the mass of the neutron star. Therefore, the gravitational field in which the neutrino-heated matter moves can be treated as a fixed-background Schwarzschild metric. Time variations of the temperature and density are then solved by use of relations based on baryon, momentum, and energy conservation (eqs. [1]–[3] in Wanajo et al. 2001). The source term in the equation of energy conservation is due to both heating and cooling by neutrino interactions. The gravitational redshift of the neutrino energies and the bending of the neutrino trajectories expected from general relativistic effects are explicitly taken into account.

For the cooling by annihilation of electron-positron pairs into neutrino-antineutrino pairs, the accurate table of Itoh et al. (1996) is utilized. All other neutrino heating and cooling rates are taken from Otsuki et al. (2000). The neutrino luminosities, L_ν, of all neutrino flavors are assumed to be equal, and the rms average neutrino energies are taken to be 12, 22, and 34 MeV, for electron, antielectron, and the other flavors of neutrinos, respectively. The equation of state for the electron and positron gas includes arbitrary relativistic pairs, which are of importance during α-processing. The electron fraction is set to be $Y_e \approx 0.43$, which was mainly determined by the equilibrium of neutrino capture on free nucleons with the above luminosities and energies of the electron and antielectron neutrinos at the neutrino sphere.

In this paper a *freezeout temperature*, T_f, is introduced to specify the final temperature of the neutrino winds. As can be seen in realistic hydrodynamic simulations of neutrino winds, all trajectories specific to the *r*-process asymptotically approach the same temperature in the stalled shock (Woosley et al. 1994). As discussed in § 3, this assumption is also reasonable from the nucleosynthetic point of view. Otsuki et al. (2000) set the mass ejection rate, $\dot{M}$, at the neutrino sphere of each wind so that the temperature at 10,000 km in radius is 0.1 MeV. This assumption may be inadequate, as the physical conditions of the neutrino sphere and the outer boundary are not necessarily causally connected. On the other hand, Wanajo et al. (2001) set the mass ejection rate to be $\dot{M} = 0.995 \times \dot{M}_c$, where $\dot{M}_c$ is the maximum mass ejection rate at the neutrino sphere appropriate for the local physical conditions (the wind with $\dot{M}_c$ becomes supersonic through the sonic point, while those with $\dot{M} < \dot{M}_c$ are subsonic throughout). However, the asymptotic temperatures differed significantly from wind to wind, which is unlikely in a realistic situation. In this paper, therefore, we have specified both $\dot{M}$ and T_f to avoid the above problems. The mass ejection rate is set to be $\dot{M} = \dot{M}_c$. In fact, recent hydrodynamic simulations show that the winds become supersonic, and then, in turn, decelerate to become subsonic from the effects of the reverse shock coming from the outer iron mantle (Burrows, Hayes, & Fryxell 1995). T_f is set to be the same for all winds. The temperature, T, of each wind is thus replaced with T_f for all $T < T_f$. The density is also replaced to that obtained at $T = T_f$. The value of T_f is determined in § 3.

3. THE *r*-PROCESS

The *r*-process nucleosynthesis calculation, adopting the model described above for the physical conditions, is obtained by application of an extensive nuclear-reaction network code. The network consists of ~ 3600 species, all the way from single neutrons and protons up to the fermium isotopes ($Z = 100$; see Fig. 2). We include all relevant reactions, i.e., (n,γ), (p,γ), (α,γ), (p,n), (α,p), (α,n), and their inverses. Reaction rates are taken from F.-K. Thielemann (1995, private communication) for nuclei with $Z \leq 46$ and from Cowan, Thielemann, & Truran (1991) for those with $Z \geq 47$. The latter used the mass formula by Hilf, van Groote, & Takahashi (1976).

Our network does not include the nuclei near the neutron drip line for $Z < 10$, since no reliable data are yet available. Terasawa et al. (2001) demonstrated that *r*-processing was hindered significantly by reaction flows near the neutron drip line for $Z < 10$, owing to their rather low asymptotic temperature ($=6.2 \times 10^8$ K). As we suggest below, however, it may be unlikely that the asymptotic temperature is, in

reality, less than $\sim 8 \times 10^8$ K. Thus, inclusion of these reactions would not significantly change our conclusions.

The three-body reaction $\alpha(\alpha n, \gamma)^9$Be, which is of special importance as the bottleneck reaction to heavier nuclei, is taken from the recent experimental data of Utsunomiya et al. (2001). The weak interactions, such as β-decay, β-delayed neutron emission (up to three neutrons), and electron capture, are also included, although the latter is found to be unimportant. Note that neutrino-induced reactions are not included. In fact, neutrino capture on free nucleons might be of importance, as they may serve to increase the electron fraction during seed element production (Meyer, McLaughlin, & Fuller 1998), while those on heavy nuclei are likely to be unimportant. However, it would be meaningless to consider these effects without taking the accurate treatment of neutrino transport near the neutrino sphere into account.

The α-decay chains and spontaneous fission processes are taken into account only after the freezeout of all other reactions. For the latter, all nuclei with $A \geq 256$ are assumed to decay by spontaneous fission only. The few known nuclei undergoing spontaneous fission for $A < 256$ are also included, along with their branching ratios. Neutron-induced and β-delayed fissions, as well as the contribution of fission fragments to the lighter nuclei, are neglected. Obviously, these treatments of the fission reactions are oversimplified. Nevertheless, this may be acceptable, at least to first order, as we demonstrate below. We leave the more accurate treatment of these matters to future work. In particular, β-delayed fission may be of importance, as shown by Schatz et al. (2002).

Each calculation is started at $T_9 = 9$ (where $T_9 \equiv T/10^9$ K). At this point the nuclear statistical equilibrium (NSE) consists mostly of free nucleons. The initial mass fractions of neutrons and protons are thus given by $X_n = 1 - Y_e$ and $X_p = Y_e$, respectively. In Wanajo et al. (2001), the initial electron fraction Y_e was fixed to be 0.40. In this paper Y_e is varied from 0.39 to 0.49 to examine its effect on the r-process. Note that, for simplicity, for each Y_e the same trajectories are used, being derived with $Y_e \approx 0.43$. The small change of Y_e is, however, found to be unimportant for the temperature and density histories.

The freezeout temperature, T_f, is determined as follows. At present, there is no positive evidence that the r-process pattern between the r-process-enhanced stars (e.g., CS 31082-001) and the solar abundances differs for $Z \geq 56$, except for Th and U (Hill et al. 2002). Thus, since our main goal is to estimate reliable yields of U and Th, the local r-process pattern near the third peak (^{195}Pt) is treated most carefully, in order to reproduce the solar r-process pattern. In Figure 1 the nucleosynthesis results before and after α-decay and fission (*thick line*), obtained with different $T_{9f} (\equiv T_f/10^9$ K), are compared to the solar r-process pattern (*dots*; Käppeler, Beer, & Wisshak 1989) normalized to

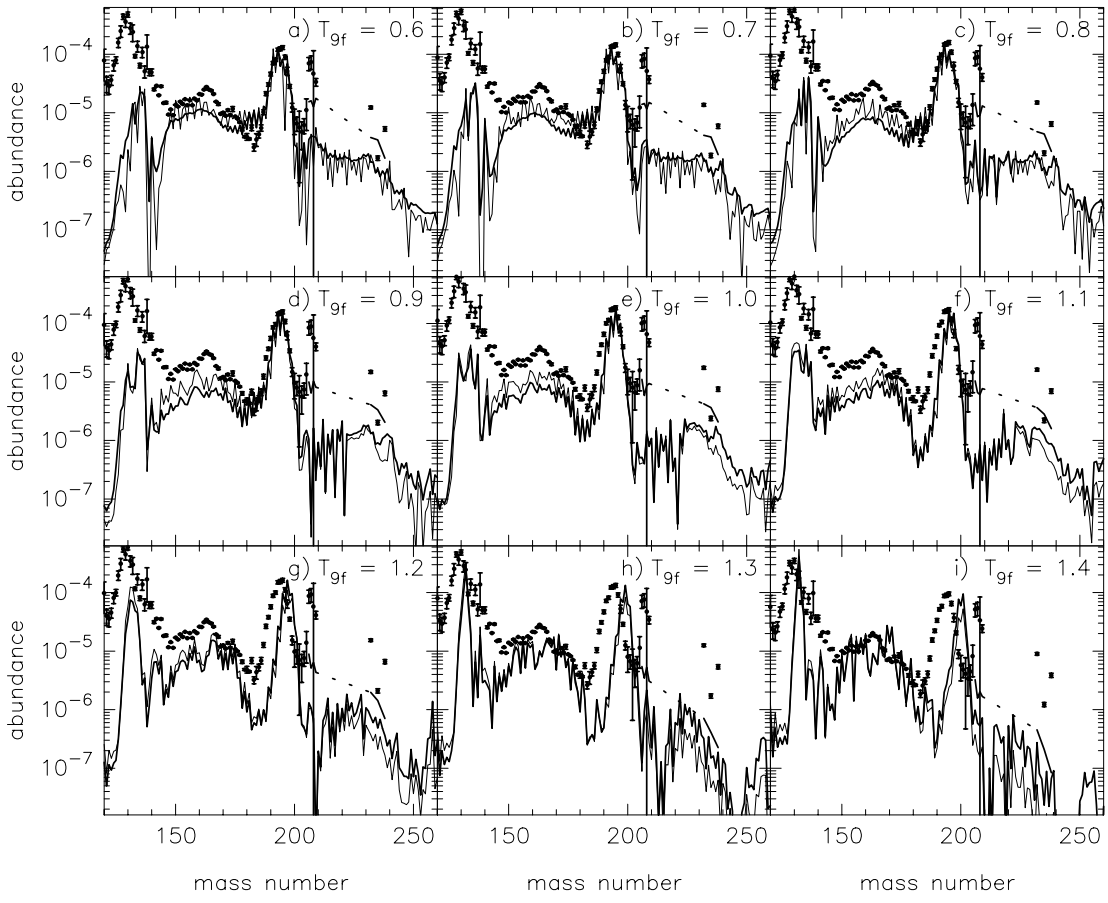

FIG. 1.—Comparison of the nucleosynthesis yields (*lines*) for $T_f =$ (*a*) 0.6, (*b*) 0.7, (*c*) 0.8, (*d*) 0.9, (*e*) 1.0, (*f*) 1.1, (*g*) 1.2, (*h*) 1.3, and (*i*) 1.4, with the solar r-pattern (*dots*), scaled at the height of the third peak for $\log L_\nu$ (ergs s^{-1}) = 51.8 with $Y_e = 0.43$. The thick and thin lines represent situations with and without β-delayed neutron emission, respectively. [*See the electronic edition of the Journal for a color version of this figure.*]

the height of the third-peak nuclei. The values of L_ν and Y_e are taken to be $10^{51.8}$ ergs s^{-1} and 0.43, respectively. The thin line denotes the results obtained by turning off the process of β-delayed neutron emission. Note that the local pattern of the r-element abundances (i.e., near $A = 195$) is not significantly altered as the result of changing L_ν and Y_e (see Figs. 4 and 5). Thus, the discussion below may hold even for superposition of the yields from multiple trajectories.

For $T_{9f} = 0.6$–0.8 (Figs. 1*a*–1*c*), the position of the third peak shifts to the low side by two units from $A = 195$. Moreover, the valley on the lower side of the third peak seen in the solar r-process pattern ($A \approx 183$) is substantially filled up with the jagged pattern. On the other hand, for $T_{9f} = 1.2$–1.4 (Figs. 1*g*–1*i*), the third peak significantly shifts to the high side from $A = 195$. In addition, the abundance pattern is unacceptably jagged compared to the solar r-process pattern. In this regard, the results with $T_{9f} = 0.9$–1.1 reproduce the properties of the solar r-pattern near the third peak quite well (Figs. 1*d*–1*f*). Indeed, the third peak is correctly located at $A = 195$. The pattern in the valley at $A \approx 183$ is also reasonably reproduced. In this paper, therefore, we set T_{9f} to be 1.0, so that the predicted r-process pattern is in the best agreement with that of the solar r-process pattern near the third peak. Note that the second peak ($A = 130$) nuclei in Figure 1 are substantially underproduced compared to the solar r-abundances in this specific trajectory, which originates mainly from the higher L_ν trajectories (Figs. 4 and 5).

In Table 1, the abundance ratios among Eu, Ir, Pb, Bi, Th, and U are listed along with the isotope number fraction of ^{151}Eu. Note that, in this table, "Pb" means the sum of ^{206}Pb, ^{207}Pb, ^{208}Pb, and ^{235}U, while "U" means ^{238}U, owing to the short mean half-life of ^{235}U compared to the cosmic age. As can be seen, the ratio U/Th is insensitive to the change of T_{9f}, except for the higher temperature cases with $T_{9f} \geq 1.2$. This is simply due to the fact that Th and U are close to one another in mass number. Thus, small variations of T_{9f} from 1.0 may not change the chronometric ages substantially, as long as the U-Th pair is employed. In contrast, other abundance ratios are found to be quite sensitive to the change of T_{9f}. For example, the ratio Th/Eu varies by more than a factor of 2 in the same temperature range. This implies that the chronometer pairs Th-r may be unreliable unless the astrophysical model is strictly constrained. It is interesting to note that the ratio between Pb-Bi and Th-U can be changed by a factor of 2 even though they are mainly α-decay products.

The isotope ratio of Eu can provide another constraint on the determination of T_{9f}. Recent spectroscopic studies have shown that the isotope number fractions of a few extremely metal poor stars, including CS 22892-052 (Sneden et al. 2002) and CS 31082-001 (W. Aoki et al., in preparation) are close to the solar value of 0.478. This is also in good agreement with the calculated values for $T_{9f} \lesssim 1.0$ in the last column of Table 1.

The strong influence of T_f on the final predicted r-process pattern can be recognized as the consequence of the freezeout effects. Figure 2 shows the postfreezeout evolution of the r-process abundances for $T_{9f} = 1.0$ with $L_\nu = 10^{51.8}$ ergs s^{-1} and $Y_e = 0.43$. The abundances are color-coded with their pattern as a function of mass number in the upper left. The dots denote the nuclei included in the reaction network, with the stable and long-lived nuclei shown as larger dots. At the freezeout of r-processing, which occurs 0.48 s after $T_9 = 9$, a clear odd-even effect appears, owing to the (n, γ)-(γ, n) equilibrium (Fig. 2*a*). After 0.58 s, the abundances near the third peak are still along the neutron magic number $N = 126$ (Fig. 2*b*). As a result, the third peak slightly shifts to the larger side in mass number, owing to the small fraction of neutrons emitted by photodissociation of fragile nuclei (e.g., $A \sim 183$) and by the β-delayed process; these are quickly absorbed by other nuclei (including those near the third peak). The abundance valley at $A \approx 183$ is then sharpened. At the same time the abundance pattern is significantly smoothed. At some point the abundances near the third peak separate from $N = 126$ as a result of β-decay, becoming more and more robust against photodissociation, as well as with the decrease in the β-delayed process (Fig. 2*c*). The position of the third peak is thus fixed. The abundance pattern is smoothed further by the continuation of nonequilibrium neutron emission and absorption among fragile nuclei. It is important to note that the separation from the $N = 126$ line takes place at earlier times for lower T_f, and vice versa, which determines the location of the third peak, as well as the smoothness of the pattern near it. Although the β-delayed process is found to be unimportant for setting the locations of the second ($A \approx 130$) and the third ($A \approx 195$) peaks, it does contribute to the enhancement of nuclei with $A > 220$, in particular for $T_{9f} \geq 0.9$, as can be seen in Figure 1. This results in the enhancement of Th-U/Pb-Bi for $T_{9f} \sim 1.0$ found in Table 1.

In order to calculate the mass-integrated r-process yields, the time evolution of the neutrino luminosity, L_ν, is assumed to be $L_\nu(t) = L_{\nu 0}(t/t_0)^{-1}$. $L_{\nu 0}$ and t_0 are taken to

TABLE 1

ABUNDANCE RATIOS

T_{9f}	Th/Eu	Th/Ir	Th/Pb[a]	Th/Bi	U/Eu[a]	U/Ir[a]	U/Pb[a]	U/Bi[a]	U/Th[a]	$f(^{151}\mathrm{Eu})$[b]
0.60.....	0.24	0.02	0.08	0.21	0.11	0.01	0.04	0.10	0.44	0.47
0.70.....	0.36	0.02	0.09	0.27	0.17	0.01	0.04	0.13	0.47	0.46
0.80.....	0.55	0.02	0.13	0.36	0.25	0.01	0.06	0.17	0.46	0.45
0.90.....	0.46	0.02	0.14	0.50	0.23	0.01	0.07	0.25	0.50	0.44
1.00.....	0.38	0.02	0.15	0.45	0.19	0.01	0.07	0.22	0.49	0.52
1.10.....	0.41	0.03	0.14	0.47	0.18	0.02	0.06	0.21	0.44	0.41
1.20.....	0.17	0.06	0.09	0.46	0.06	0.02	0.03	0.16	0.36	0.40
1.30.....	0.05	0.09	0.05	0.23	0.01	0.03	0.02	0.07	0.32	0.24
1.40.....	0.03	0.15	0.06	0.27	0.01	0.03	0.01	0.05	0.18	0.19

[a] Pb = ^{206}Pb + ^{207}Pb + ^{208} Pb + ^{235} U, U = ^{238}U (see text)

[b] Isotope number fraction of ^{151}Eu.

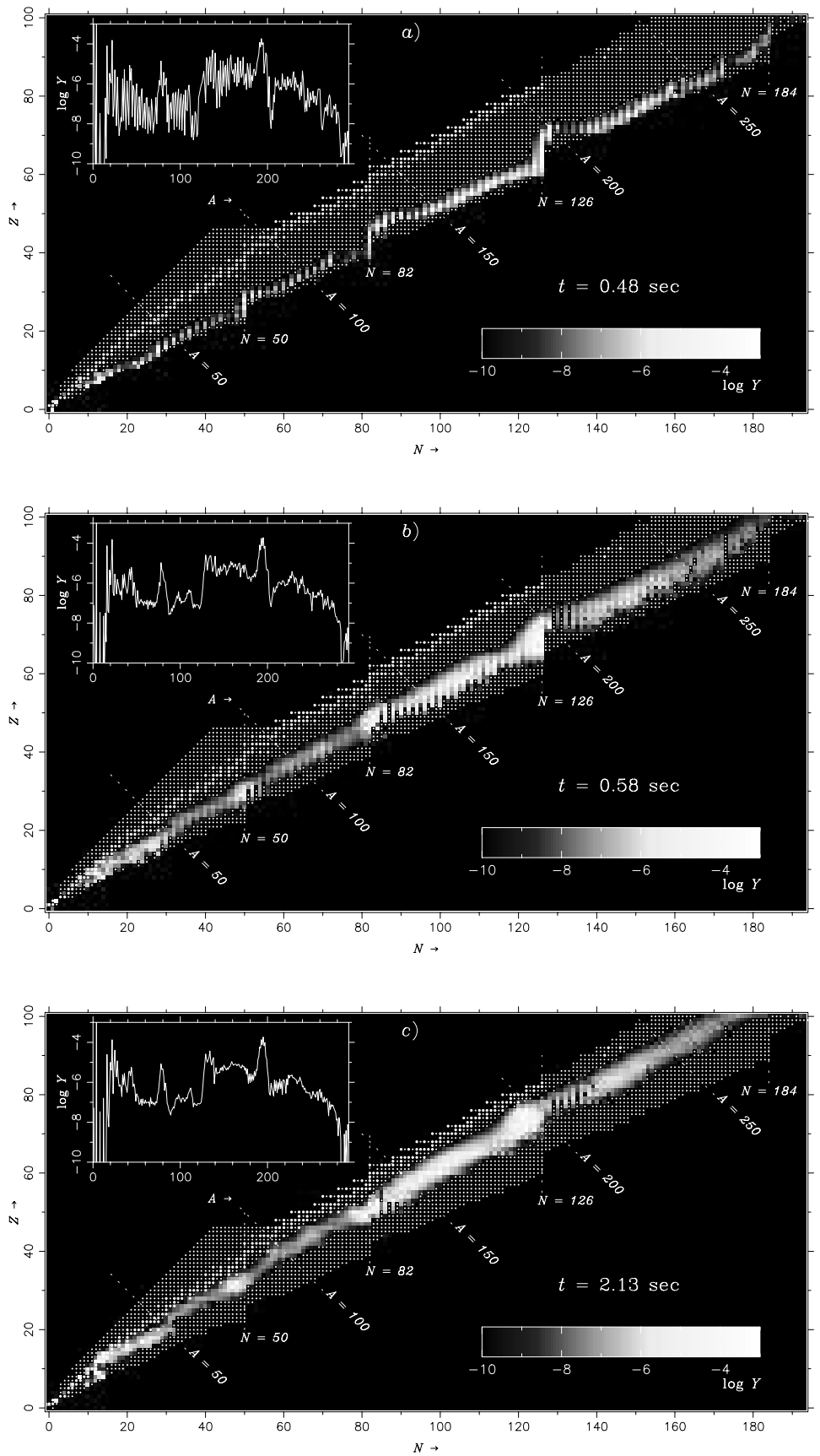

FIG. 2.—Postfreezout evolution of the *r*-process yields at $t = (a)$ 0.48, (b) 0.58, and (c) 2.13 s for $\log L_\nu$ (ergs s^{-1}) = 51.8 and $Y_e = 0.43$. The abundances are color-coded in the nuclide chart. The pattern as a function of mass number is shown in the upper left of each panel. The nuclei included in the reaction network are denoted by dots, with the stable and long-lived isotopes represented by large dots. [*See the electronic edition of the Journal for a color version of this figure.*]

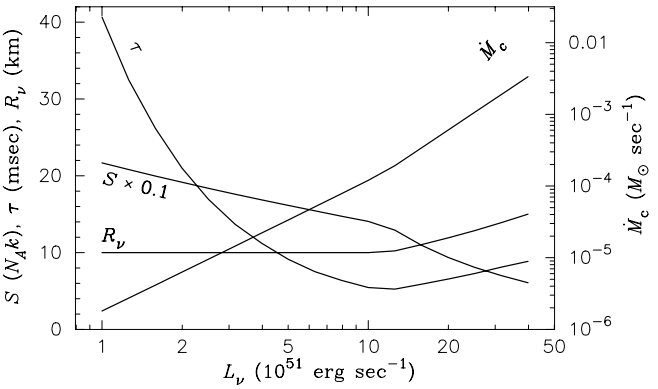

FIG. 3.—Entropy per baryon (S), timescale of the seed production (τ), neutrino sphere radius (R_ν), and mass ejection rate ($\dot{M}_c$) as functions of the neutrino luminosity (L_ν), in units denoted along the axes.

be $10^{52.6}$ ergs s^{-1} ($\approx 4 \times 10^{52}$ ergs s^{-1}) and 0.2 s, respectively, being in reasonable agreement with the hydrodynamic results of Woosley et al. (1994). The time evolution of the neutrino sphere radius is also assumed to be $R_\nu(t) = R_{\nu 0}(t/t_0)^{-1/3}$, where $R_{\nu 0} = 15$ km; R_ν is replaced with 10 km for $R_\nu < 10$ km. This rather rapid contraction of R_ν is required for robust *r*-processing to occur at early times with a compact proto–neutron star model (Wanajo et al. 2001; Thompson et al. 2001). Figure 3 shows R_ν (km) and $\dot{M}_c$ ($M_\odot$ s^{-1}), as well as the entropy per baryon S ($N_A k$) and the timescale of seed abundance production τ (ms), as functions of L_ν. The timescale, τ, is defined as the duration from 6 to 2.5 in T_9, which approximately corresponds to the phase of α-processing, i.e., the seed abundance production prior to *r*-processing. Note that our definition of τ differs from the *e*-folding time of the density often taken in other work, since the latter is not necessarily a good indicator of the seed abundance production. For $L_\nu \approx 5$–10×10^{51} ergs s^{-1}, τ is significantly short ($\approx$5–10 ms) and S is moderately high ($\approx 140 N_A k$–$160 N_A k$), which are suitable conditions for the *r*-process (preventing consumption of free neutrons prior to *r*-processing). For $L_\nu \gtrsim 10^{52}$ ergs s^{-1}, τ increases and S decreases rapidly with L_ν, owing to the increasing R_ν. The total ejected mass, calculated by following the time evolution of L_ν and $\dot{M}_c$, is $5.0 \times 10^{-4}\ M_\odot$, more than 1 order of magnitude smaller than that of Woosley et al. (1994). This is perhaps due to the fact that our assumption of the steady state flow does not hold well for $L_\nu > 10^{52}$ ergs s^{-1}. This high-luminosity phase is, however, unimportant for the *r*-process (Fig. 4).

The nucleosynthesis results for different L_ν with $Y_e = 0.43$, before α-decay and spontaneous fission, are shown in Figure 4. For $\log L_\nu(\text{ergs s}^{-1}) = 52.6$, 52.4, and 52.2, no significant *r*-processing beyond the second peak occurs (Figs. 4*a*–4*c*). This is due to the low S ($=61 N_A k$, $81 N_A k$, and $110 N_A k$), regardless of the short τ (=8.9, 7.3, 5.9 ms). For $\log L_\nu(\text{ergs s}^{-1}) = 52.0$, 51.8, and 51.6, robust *r*-processing occurs, producing the second- and third-peak nuclei and substantial actinides (Figs. 4*d*–4*f*). This is a consequence of the rather short timescale of seed abundance production ($\tau = 5.5$, 7.5, 11 ms) and the high entropy per baryon ($S = 141 N_A k$, $154 N_A k$, and $169 N_A k$). For $\log L_\nu(\text{ergs s}^{-1}) = 51.4$, 51.2, and 51.0, the second and the third peaks are still prominent, but production of the actinides is not of importance with high S ($=184 N_A k$, $200 N_A k$,

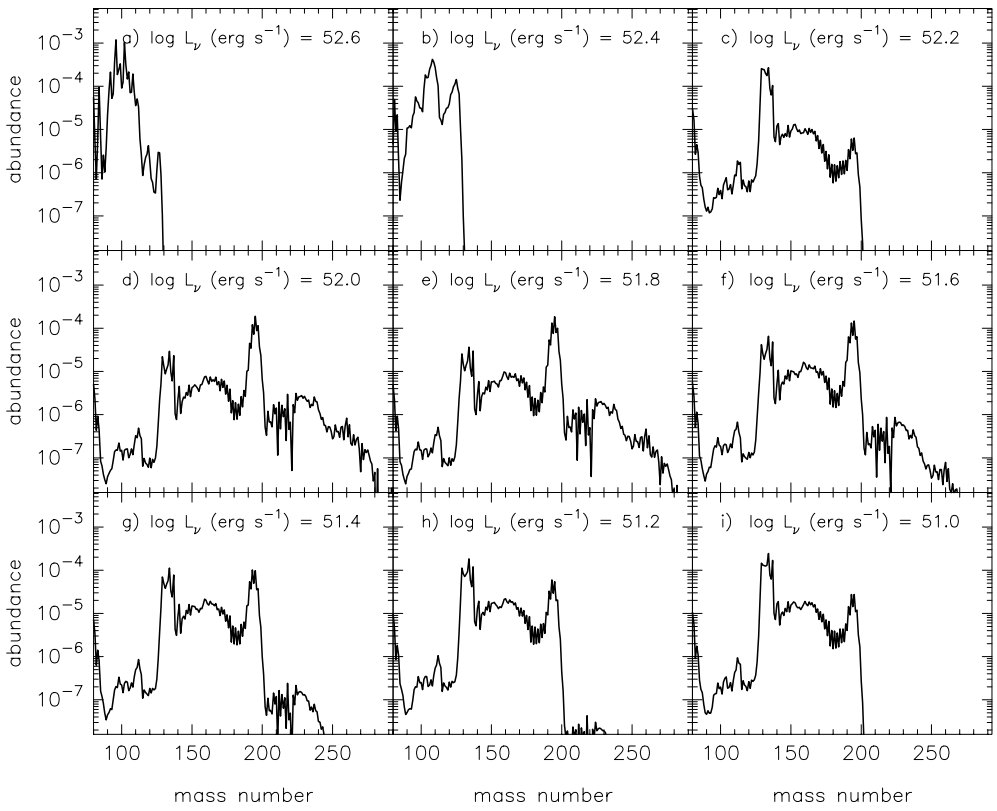

FIG. 4.—Calculated yields for $\log L_\nu$ (ergs s^{-1}) = (*a*) 52.6, (*b*) 52.4, (*c*) 52.2, (*d*) 52.0, (*e*) 51.8, (*f*) 51.6, (*g*) 51.4, (*h*) 51.2, and (*i*) 51.0, with $Y_e = 0.43$

$217N_A k$) and long τ (=17, 26, and 41 ms; Figs. 4*g*–4*h*). Note that, for $\log L_\nu(\mathrm{ergs\ s^{-1}}) = 52.0$–51.0, the positions of the second ($A \approx 130$) and third ($A \approx 195$) peaks and the valley at $A \approx 183$ do not vary significantly (nor do the local patterns close to these features), although the global patterns are different (Figs. *4d*–4*i*). This is due to the use of the same T_f ($=1.0 \times 10^9$ K) in all situations.

We now integrate the nucleosynthesis results of trajectories with $\log L_\nu(\mathrm{ergs\ s^{-1}}) = 52.6$–51.0, using the time evolution of L_ν with $\dot{M}_c$ (Fig. 3). The interval of L_ν is taken to be 0.1 dex. These L_ν correspond to times $t = 0.2$–8.0 s at the neutrino sphere. The abundances of species formed after this period are neglected because of the small $\dot{M}_c$ ($<2 \times 10^{-6}\ M_\odot\ \mathrm{s^{-1}}$). In Figure 5 the mass-integrated abundances are compared with the solar *r*-process pattern (Käppeler et al. 1989) scaled to match ^{153}Eu. The α-decay and spontaneous fission after freezeout of all other reactions are included. The initial electron fraction, Y_e, is varied from 0.39 to 0.49 to demonstrate its effect on the *r*-process. Note that in our models Y_e is taken to be constant with time. Although Y_e should certainly be a function of time, it is meaningless to consider this refinement without taking into account accurate treatment of neutrino transport near the neutrino sphere. As can be seen in Figure 5, for $Y_e = 0.39$–0.43, the calculated abundances are in reasonable agreement with the solar *r*-process pattern between $A \approx 120$ and 200. For larger neutron excess, with $Y_e = 0.39$–0.41, ^{232}Th and ^{235,238}U are significantly overproduced compared to the solar *r*-process pattern (Figs. 5*a*–5*c*), as are other (stable) nuclei near the third peak. For $Y_e = 0.42$, overall agreement of the abundance pattern of $A \geq 120$ to the solar *r*-process pattern can be seen (Fig. 5*d*). For $Y_e = 0.43$, Th and U are significantly underproduced compared to the solar *r*-process pattern (Fig. 5*e*). In the current models, therefore, Y_e should be ≤ 0.42 to achieve sufficient production of Th and U. Note that the location of the third ($A \approx 195$) peak and the valley at $A \approx 183$ still hold even after integration of the yields. The deficiency of nuclei at $A = 130$–140, seen for all Y_e cases, could be due to our insufficient treatment of the physics of the neutrino winds for $L_\nu > 10^{52}$ ergs s^{-1}, in which the assumption of the steady state winds is not manifest at all. More likely, this might be due to the nuclear properties of the mass model (Hilf et al. 1976) employed in this study, as shown by Freiburghaus et al. (1999a). In their paper, calculations with other mass formulae, FRDM (Möller et al. 1995) and ETFSI (Aboussir et

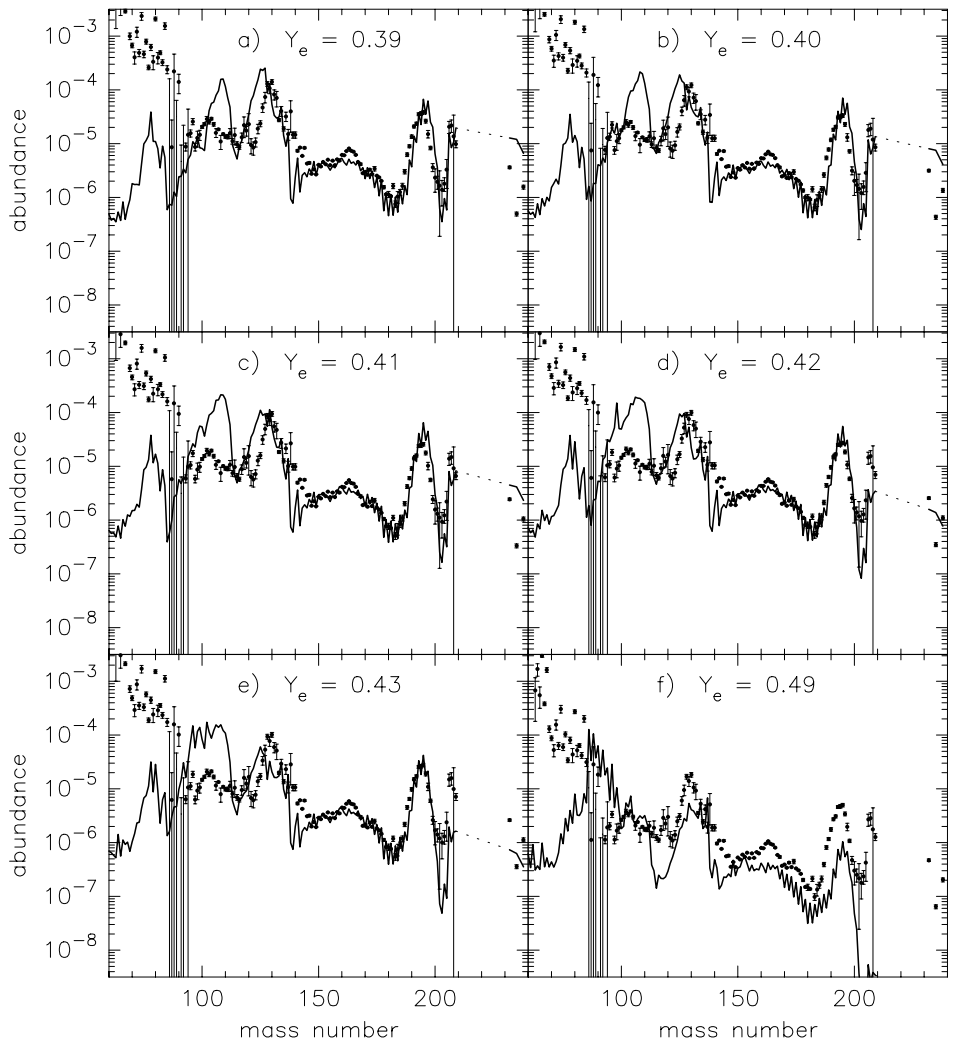

FIG. 5.—Comparison of the mass-integrated yields (*lines*) for $Y_e = (a)$ 0.39, (*b*) 0.40, (*c*) 0.41, (*d*) 0.42, (*e*) 0.43, and (*f*) 0.49 with the solar *r*-pattern (*dots*) scaled at ^{153}Eu, as functions of mass number. [*See the electronic edition of the Journal for a color version of this figure.*]

al. 1995), were able to well reproduce the solar *r*-abundances in this mass region.

As can be seen in Figure 5, overproduction of nuclei with $A \approx 90$–110 is evident, except for the $Y_e = 0.49$ case. This is a consequence of the large $\dot{M}_c$ for $L_\nu > 10^{52}$ ergs s^{-1} (Fig. 3), in which little *r*-processing occurs (Figs. 4*a*–4*c*). For high Y_e (=0.49, Fig. 5*f*), the overproduction significantly diminishes. This arises because, in the nuclide chart (see Fig. 2), $Y_{e,\,\mathrm{seed}} > 0.446$ lines have intersections with α separation energies of ≈6 MeV on the lower side of the neutron magic number $N = 50$ (Hoffman et al. 1996; Freiburghaus et al. 1999a). At the same time, however, the *r*-process abundance of $A \approx 120$–200 decreases substantially. This is due to the small levels of the seed abundance, owing to the extremely strong α-rich freezeout by the less efficient $\alpha(\alpha n, \gamma)^9$Be reaction with low neutron excess (Hoffman, Woosley, & Qian 1997).

In Table 2 the total ejected masses of *r*-process abundances ($A \geq 120$) are shown, along with that of Eu. For $Y_e = 0.49$, the ejected mass is about 1 order of magnitude smaller than for other Y_e cases. According to the chemical evolution study of the Galactic halo by Ishimaru & Wanajo (1999), $\sim 5 \times 10^{-7}\ M_\odot$ of Eu per *r*-process event is needed to reproduce the large dispersion of observed Eu/Fe in extremely metal poor stars. The mass of Eu obtained for $Y_e = 0.49$ is too small compared to that level while remaining in reasonable agreement for lower Y_e cases. We speculate that, if the primary *r*-process site is *really* neutrino winds, as discussed in this study, the electron fraction changes from $Y_e \approx 0.49$ to $\lesssim 0.42$ rapidly with time. In this case, the overproduction would not appear at the early phase ($L_\nu > 10^{52}$ ergs s^{-1}) but would be followed by later *r*-nuclei ($A > 120$) production ($L_\nu < 10^{52}$ ergs s^{-1}). As can be seen in the third column in Table 2, except for $Y_e = 0.49$, the isotopic fraction of ^{151}Eu is in good agreement with both the solar value and the observational estimates (Sneden et al. 2002; W. Aoki et al., in preparation), even after mass-integration of the yields.

The last column of Table 2 shows the mass of fission fragments, whose contribution to the lighter nuclei is neglected in this study. This assumption appears adequate since the contribution of fission fragments is less than 5% of the total mass of nuclei with $A \geq 120$. This follows since, in this study, the neutron-to-seed ratio at the onset of *r*-processing ($T_9 = 2.5$) is 138 at most, with $\langle A_{\mathrm{seed}} \rangle \approx 95$. This results in no significant production of nuclei with $A \geq 255$, where fission dominates.

TABLE 2
EJECTED MASS ($M_\odot$)

Y_e	$A \geq 120$	Eu	$f(^{151}\mathrm{Eu})$[a]	Fission[b]
0.39.....	1.5×10^{-4}	6.2×10^{-7}	0.50	0.042
0.40.....	1.2×10^{-4}	5.4×10^{-7}	0.50	0.025
0.41.....	9.5×10^{-5}	4.3×10^{-7}	0.52	0.014
0.42.....	7.4×10^{-5}	4.5×10^{-7}	0.51	0.005
0.43.....	5.6×10^{-5}	4.6×10^{-7}	0.51	0.002
0.49.....	4.5×10^{-6}	6.8×10^{-8}	0.40	0.000

[a] Isotope number fraction of ^{151}Eu.
[b] Mass fraction of fission fragments ($A \geq 120$).

4. THE U-Th COSMOCHRONOLOGY

In Figure 6 the available spectroscopic abundance data for CS 31082-001 (*dots*) are compared with the nucleosynthesis results discussed in § 3 (*thick lines*) and with the solar *r*-pattern (*thin lines*), scaled at Eu ($Z = 63$). The data for the neutron-capture elements in this star are taken from Hill et al. (2002). CS 31082-001 is the first extremely metal poor star ([Fe/H] = −2.9) in which the U II line (3859.59 Å) has been detected (Cayrel et al. 2001). The abundance pattern of this star between Ba ($Z = 56$) and Ir ($Z = 77$) is in excellent agreement with the solar *r*-process pattern, except for a few elements (Tb, Hf, Os). It is possible that, in these few cases, the disagreements are due to difficulties in the abundance estimates (Hill et al. 2002). Note that some lighter elements (Rh, Ag) are not in agreement with the solar *r*-process pattern, as has also been seen in CS 22892-052 (Sneden et al. 2000), which implies the presence of two distinct *r*-process sites (Ishimaru & Wanajo 2000; Qian 2000).

Nucleosynthesis results for all Y_e cases are in good agreement with the abundance pattern of CS 31082-001 for the elements between Pr ($Z = 59$) and Tm ($Z = 69$), with the exception of Tb. Note that a few of the predicted abundances for elements near the second peak (Ba, La, and Ce) are significantly deficient compared to both the observational and solar patterns. As mentioned in § 3, this might be due to the properties of the nuclear mass model employed in this study. In future work we plan to check whether these elements are reproduced with other mass formulae, since the observational data suggest the universality of the *r*-process pattern between the second and the third *r*-process peaks. The platinum-peak elements Os and Ir are in reasonable agreement, except for the $Y_e = 0.49$ case, although the height of the ^{195}Pt differs. In addition, the large abundance of Os in CS 31082-001 compared to the scaled solar *r*-process pattern makes it questionable if the third peak is really located at Pt. It would clearly be useful to obtain measurements of the Pt abundance in this star, so that the height, as well as the position, of the third peak could be better constrained. Note that ^{235}U is assumed to have α-decayed away because of its relatively short half life (0.704 Gyr).

As discussed by Hill et al. (2002), the age of CS 31082-001 can be inferred by application of one or more of the following three relations:

$$t^*_{\mathrm{Th},r} = 46.67\ [\log(\mathrm{Th}/r)_0 - \log(\mathrm{Th}/r)_{\mathrm{now}}]\ \mathrm{Gyr}\ , \quad (1)$$

$$t^*_{\mathrm{U},r} = 14.84\ [\log(\mathrm{U}/r)_0 - \log(\mathrm{U}/r)_{\mathrm{now}}]\ \mathrm{Gyr}\ , \quad (2)$$

$$t^*_{\mathrm{U,Th}} = 21.76\ [\log(\mathrm{U}/\mathrm{Th})_0 - \log(\mathrm{U}/\mathrm{Th})_{\mathrm{now}}]\ \mathrm{Gyr}\ , \quad (3)$$

with the half-lives of ^{232}Th (14.05 Gyr) and ^{238}U (4.468 Gyr), where *r* is a stable *r*-element and the subscripts "0" and "now" denote the initial and current values derived by theory and observation, respectively. In principle, $t^*_{\mathrm{U},r}$ and $t^*_{\mathrm{U,Th}}$ can be more precise chronometers than $t^*_{\mathrm{Th},r}$, owing to the smaller coefficients in front of equations (2) and (3). In practice, the U-Th pair (eq. [3]) is expected to be the most precise chronometer owing to the similar atomic properties of these species, which serve to diminish the observational errors associated with determination of their ratio. Furthermore, the ratio U/Th is less dependant on the theoretical model used, since these species are separated by only two units in atomic number, as well as being mostly the result of α-decayed products (Table 1). As stable elements *r*, Eu, Os, and Ir are selected. The Eu abundance derived by spectro-

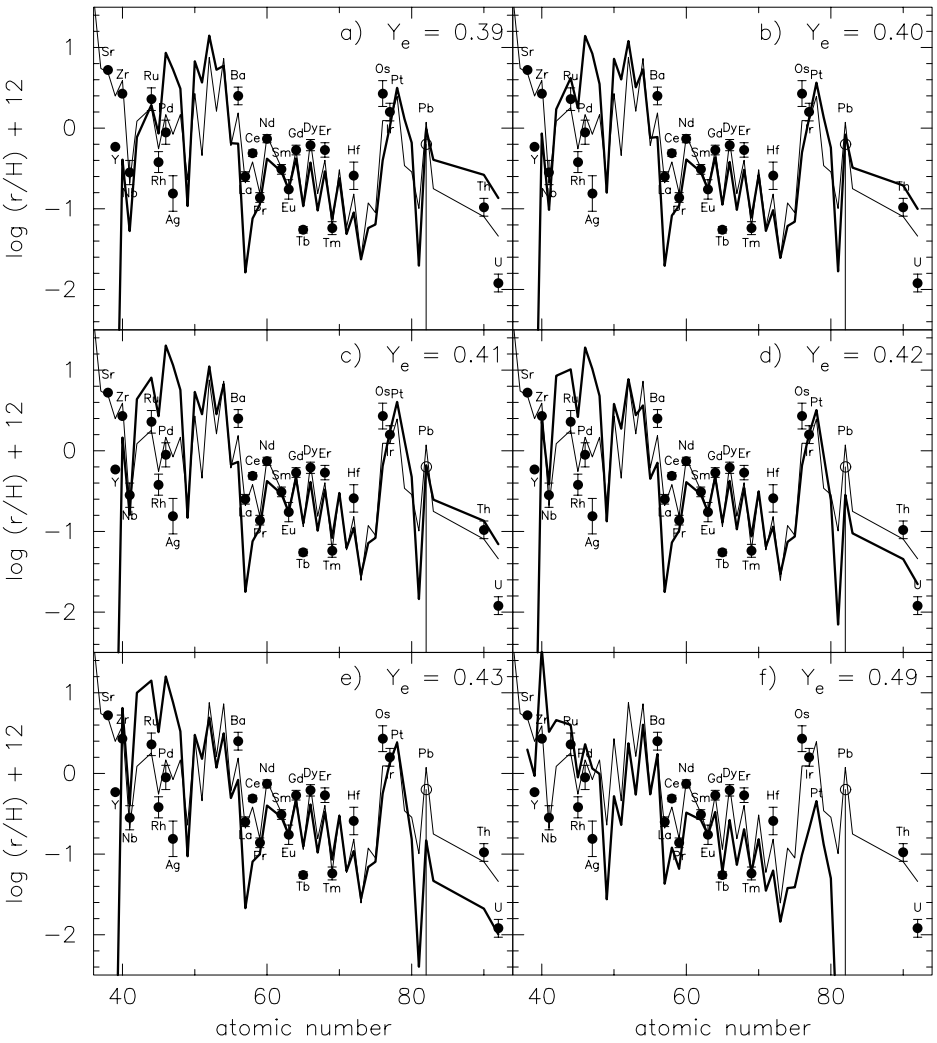

FIG. 6.—Comparison of the mass-integrated yields (*thick line*) for $Y_e = (a)$ 0.39, (*b*) 0.40, (*c*) 0.41, (*d*) 0.42, (*e*) 0.43, and (*f*) 0.49, scaled at Eu ($Z = 63$), with the abundance pattern of CS 31082-001 (*filled circles, with observational error bars*), as functions of atomic number. For Pb, the observed upper limit is shown by the open circle. The scaled solar *r*-pattern is shown by the thin line. [*See the electronic edition of the Journal for a color version of this figure.*]

scopic analyses is more reliable than for any other elements with $Z \geq 59$. The Pt-peak elements Os and Ir are coproduced with Th and U in the same (or close in L_ν) trajectories, and thus they are perhaps less model-dependent as well. Note that, if possible, the Pb abundance in this star should be used, since it is mainly synthesized by the same α-decay chains as Th and U. However, Pb has not yet been detected in CS 31082-001, and for now only an upper limit to its abundance is available. For reasons that are not yet clear, the upper bound on Pb reported by Hill et al. (2002) is lower than the solar value, being satisfied only by the $Y_e \leq 0.42$ cases in which Th and U are not significantly produced. Thus, Pb is omitted for the age determination in this study, although its future measurement would clearly be of importance.

Table 3 lists the predicted initial abundance ratios among Eu, Os, Ir, Pt, Th, and U ($A = 238$) for all the Y_e cases considered in the present study. The ratio U/Th is found to be insensitive to Y_e (except for the extreme case of $Y_e = 0.49$), which is in excellent agreement with those constrained by

TABLE 3
ABUNDANCE RATIO (LOG SCALE)

Y_e	Th/Eu	Th/Os	Th/Ir	Th/Pt	U/Eu	U/Os	U/Ir	U/Pt	U/Th
0.39...	0.18	−0.18	−0.60	−1.08	−0.11	−0.47	−0.89	−1.37	−0.29
0.40...	0.05	−0.41	−0.84	−1.27	−0.24	−0.70	−1.13	−1.57	−0.29
0.41...	−0.11	−0.68	−1.10	−1.48	−0.40	−0.97	−1.39	−1.76	−0.29
0.42...	−0.58	−1.16	−1.56	−1.85	−0.89	−1.47	−1.87	−2.16	−0.31
0.43...	−0.92	−1.43	−1.82	−2.06	−1.24	−1.75	−2.13	−2.38	−0.32
0.49...	−2.75	−2.50	−2.83	−3.17	−3.13	−2.89	−3.21	−3.55	−0.38

TABLE 4
AGES OF CS 31082-001 (GYR)

Y_e	Th/Eu	Th/Os	Th/Ir	U/Eu	U/Os	U/Ir	U/Th
0.39...	18.77	57.52	27.18	15.63	27.95	18.30	14.16
0.40...	12.61	46.73	16.09	13.62	24.47	14.73	14.10
0.41...	5.17	34.01	3.64	11.32	20.49	10.83	14.19
0.42...	−16.90	11.67	−17.55	3.97	13.05	3.76	13.70
0.43...	−32.54	−0.84	−29.64	−1.12	8.96	−0.20	13.53
0.49...	−118.21	−51.05	−76.97	−29.30	−7.94	−16.18	12.16

the solar *r*-process abundances in Goriely & Arnould (2001). It should be noted that these values can be applied not only to CS 31082-001, but also to other metal-poor halo stars in which uranium and thorium (and platinum) are detected by future observations (Cowan et al. 2002). With the use of these ratios as the initial values, the age of CS 31082-001 is derived as shown in Table 4, as well as in Figure 7. It is noteworthy that the age obtained from the U-Th chronometer pair is considerably more robust than the alternatives, resulting in a range ~13.5–14.2 Gyr, with an exception of 12.2 Gyr for the $Y_e = 0.49$ case. Therefore, we use only the U-Th chronometer for dating of this star, while the others are regarded as consistency checks only. In particular, the Th-Eu pair should be used to constrain the model parameter Y_e in this study, the species being widely separated in mass number. For this reason, Y_e is constrained to be ≈0.40, owing to the consistency between ages based on the U-Th pair and others (especially Th-Eu). The ages obtained by use of Os are significantly higher than those by others, because of the previously noted discrepancies between observation and the theoretical prediction (Fig. 6). As seen in Table 4, the difference between the ages obtained from U-Th between $Y_e = 0.39$ and 0.41 is only 0.1 Gyr. On the other hand, the observational error associated with the U/Th ratio, 0.11 dex, leads to an uncertainty of 2.4 Gyr from application of equation (3). We conclude, therefore, that the age of CS 31082-001 is 14.1 ± 2.5 Gyr.

It should be emphasized that the age determination made in the present paper is derived from the exploration of a single specific model based on the neutrino-wind scenario and relies as well on the choice of one of the many existing nuclear data sets. Thus, it is clear that our final result may be changed if we were to make use of other astrophysical models. The nuclear mass models can also significantly affect the age determination (Goriely & Arnould 2001). Obviously, more study with other astrophysical models, as well as with a number of different nuclear data sets, is needed to derive the final results.

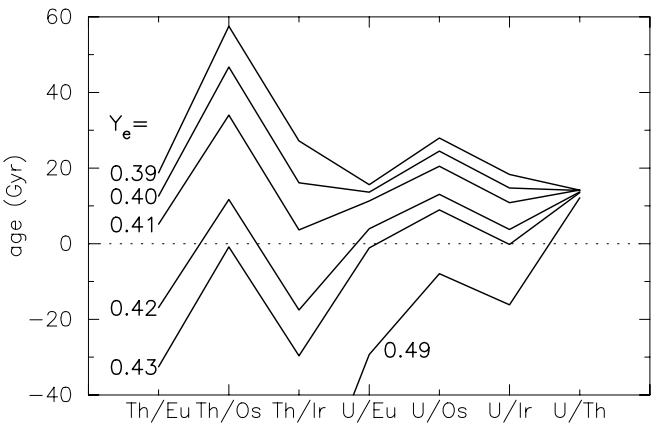

FIG. 7.—Ages of CS 31082-001 derived from various chronometer pairs. The robustness of the U-Th pair is clearly shown. The superiority of the U-*r* pairs compared to those of Th-*r* can also be seen.

5. SUMMARY AND CONCLUSIONS

We have constructed a robust model of the *r*-process based on the neutrino-wind scenario for application to the U-Th cosmochronology. The model of neutrino winds was taken from Otsuki et al. (2000) and Wanajo et al. (2001), along with some improvements described above. The *r*-process with various neutron star masses ($M_{\rm NS}$) and radii ($\approx R_\nu$) has already been explored extensively by Wanajo et al. (2001). Thus, $M_{\rm NS}$ and (asymptotic) R_ν were fixed to be 2.0 $M_\odot$ and 10 km, respectively, for which the most robust *r*-processing was realized. On the other hand, the initial electron fraction Y_e (assumed constant with time) was taken to be a free parameter, rather than fixed to be 0.40 as in Wanajo et al. (2001).

The model was tuned to fit the solar *r*-process pattern, since recent spectroscopic studies of extremely metal poor stars have indicated a *universal* (solar *r*-like) abundance pattern, at least between the second and third *r*-process peaks. Attention was paid to reproduce the pattern near $A \approx 195$, being close to Th and U in mass number. We introduced the freezeout temperature, T_f, as the most crucial parameter for constructing the model. Comparing the nucleosynthesis results with the solar *r*-process pattern, T_f was determined to be 1.0×10^9 K. The nucleosynthesis yields were mass-integrated assuming simple evolutions of L_ν and R_ν. The results between $A \approx 120$ and 200 for $Y_e = 0.39$–0.43 models were in good agreement with the solar *r*-pattern, although the production of Th and U differed from model to model.

The results of our nucleosynthesis predictions were compared to the spectroscopic abundance pattern of the *r*-process–enhanced metal-poor star CS 31082-001. Explorations of various combinations between the actinides and stable isotopes indicated that the $Y_e = 0.40$ case was found to be the best models for the age determination in this study. As a result, the age of CS 31082-001 was determined to be 14.1 ± 2.5 Gyr by use of the U-Th chronometer, which can be regarded as a hard lower limit on the age of the universe. In fact, this age is in excellent agreement with the age of the universe derived by other dating techniques (e.g., globular clusters, Type Ia supernovae, and the cosmic microwave background), as well as with other stellar radioactive age estimates using the Th-Eu (Sneden et al. 1996; Cowan et al.

1997) and U-Th (Hill et al. 2002; Schatz et al. 2002; Cowan et al. 2002) pairs. Such a strong constraint on the age of this star was only made possible by the use of U and Th in conjunction with one another. Without uranium, the chronometers involving Th alone presented only rather loose constraints.

In this study the Pb abundance in CS 31082-001 was not available for age determination, since only an upper limit on its abundance has been presented to date. It should be noted that the predicted Pb abundance for $Y_e = 0.40$ case is *higher* than this upper limit, which seems difficult to solve (Schatz et al. 2002). It is noteworthy, however, that freezeout effects can increase the ratio Th-U/Pb-Bi (see § 3), which should be examined further, as well as with other nuclear data sets. It remains possible that the solar *r*-process Pb abundance, inferred from the residual of the solar *s*-process components, is not correct (Arlandini et al. 1999). Clearly, reinvestigation of the Pb abundance in CS 31082-001, as well expansion of the searches for additional *r*-process-enhanced metal-poor stars, in which both U and Th are measurable, are highly desirable in the near future. It is also of importance to obtain measurements of the Pt abundance in CS 31082-001 (which is only possible with the strong Pt absorption features observable in the near UV from space), so as to constrain the height, as well as the position, of the third peak (Cowan et al. 2002).

We emphasize that the conclusions in this study should be considered as merely the first step toward a better understanding of the dating technique involving the U-Th chronometer. In particular, we note that the inferred age of CS 31082-001 could be significantly changed if we had utilized a different nuclear mass model, as demonstrated by Goriely & Arnould (2001). We expect, however, that a detailed comparison of the nucleosynthesis results with the solar *r*-process pattern, as in § 3, can distinguish better mass models. We suggest that the freezeout temperature, T_f (or the asymptotic temperature in more realistic models), is a useful parameter, as the freezeout effects are of importance to the final *r*-process pattern. While the waiting-point approximation, often referred to as the "classical *r*-process model," has been an effective (and thus far, the only) method used to test the nuclear mass models, we should keep in mind that nonequilibrium processes can lead to nonnegligible effects, as discussed in § 3 (e.g., the positions of the *r*-process peaks, the smoothness of abundance pattern, and the ratio Th-U/Pb-Bi).

It should also be noted that we would not insist that the neutrino-wind model explored in this study is necessarily the best (or only) astrophysical site for the *r*-process. In fact, the physical conditions in this model, namely, the rather massive proto–neutron star ($2.0\ M_\odot$) with rapid contraction of R_ν to be 10 km, seem difficult to be achieved according to the current hydrodynamic studies. Clearly, more study is needed to seek the true *r*-process site. Nevertheless, it is encouraging that the age of the CS 31082-001 determined in this study is in excellent agreement with the age of the universe derived by other dating techniques. We hope our results provide some fresh insights to the future modeling of the true astrophysical *r*-process site.

We would like to acknowledge V. Hill for providing an up-to-date abundance table for CS 31082-001 prior to publication. We also thank H. Schatz for helpful discussions and the referee, J. J. Cowan, who helped us to improve this paper. S. W. thanks K. Sumiyoshi and H. Utsunomiya for providing data for the $\alpha(\alpha, n)^9$Be reaction. This work was supported by a Grant-in-Aid for Scientific Research (13740129) from the Ministry of Education, Culture, Sports, Science, and Technology of Japan. T. C. B. acknowledges partial support from NSF grants AST 00-98549 and AST 00-98508. T. C. B. would also like to recognize partial support from an international scholar fellowship from the Ministry of Education, Culture, Sports, Science, and Technology of Japan, which supported his sabbatical stay in Tokyo, where discussions leading to the present paper were initiated.

REFERENCES

Aboussir, Y., Pearson, J. M., Dutta, A. K., & Tondeur, F. 1995, At. Data Nucl. Data Tables, 61, 127
Arlandini, C., Käppeler, F., Wisshak, K., Gallino, R., Busso, M., & Straniero, O. 1999, ApJ, 525, 886
Burrows, A., Hayes, J., & Fryxell, B. A. 1995, ApJ, 450, 830
Cardall, C. Y., & Fuller, G. M. 1997, ApJ, 486, L111
Carretta, E., Gratton, R. G., Clementini, & G., Fusi Pecci, F. 2000, ApJ, 533, 215
Cayrel, R., et al. 2001, Nature, 409, 691
Cowan, J. J., McWilliam, A., Sneden, C., & Burris, D. L. 1997, ApJ, 480, 246
Cowan, J. J., Pfeiffer, B., Kratz, K.-L., Thielemann, F.-K., Sneden, C., Burles, S., Tytler, D., & Beers, T. C. 1999, ApJ, 521, 194
Cowan, J. J., Thielemann, F.-K., & Truran, J. W. 1991, Phys. Rep., 208, 267
Cowan, J. J., et al. 2002, ApJ, 572, 861
Freiburghaus, C., Rembges, J.-F., Rauscher, T., Kolbe, E., Thielemann, F.-K., Kratz, K.-L., Pfeiffer, B., & Cowan, J. J. 1999a, ApJ, 516, 381
Freiburghaus, C., Rosswog, S., & Thielemann, F.-K. 1999b, ApJ, 525, L121
Goriely, S., & Arnould, M. 2001, A&A, 379, 1113
Goriely, S., & Clerbaux, B. 1999, A&A, 346, 798
Hilf, E. R., von Groote, H., & Takahashi, K. 1976, in Proc. Third International Conference on Nuclei Far from Stability (Geneva: CERN), 142
Hill, V., et al. 2002, A&A, 387, 560
Hoffman, R. D., Woosley, S. E., Fuller, G. M., & Meyer, B. S. 1996, ApJ, 460, 478
Hoffman, R. D., Woosley, S. E., & Qian, Y.-Z. 1997, ApJ, 482, 951
Ishimaru, Y., & Wanajo, S. 1999, ApJ, 511, L33
Ishimaru, Y., & Wanajo, S. 2000, in First Stars, ed. A. Weiss, T. Abel, & V. Hill (Berlin: Springer), 189
Itoh, N., Hayashi, H., Nishikawa, A., & Kohyama, Y. 1996, ApJS, 102, 411
Johnson, J. A., & Bolte, M. 2001, ApJ, 554, 888
Käppeler, F., Beer, H., & Wisshak, K. 1989, Rep. Prog. Phys., 52, 945
Knox, L., Christensen, N., & Skordis, C. 2001, ApJ, 563, L95
Meyer, B. S., McLaughlin, G. C., & Fuller G. M. 1998, Phys. Rev. C, 58, 3696
Möller, P., Nix, J. R., Myers, W. D., & Swiatecki, W. J. 1995, At. Data Nucl. Data Tables, 59, 131
Nilsson, H., Ivarsson, S., Johansson, S., & Lundberg, H. 2002a, A&A, 381, 1090
Nilsson, H., Zhang, Z., Lundberg, H., Johansson, S., & Nordström, B. 2002b, A&A, 381, 1090
Otsuki, K., Tagoshi, H., Kajino, T., & Wanajo, S. 2000, ApJ, 533, 424
Perlmutter, S., et al. 1999, ApJ, 517, 565
Qian, Y.-Z. 2000, ApJ, 534, L67
Qian, Y.-Z., & Woosley, S. E. 1996, ApJ, 471, 331
Schatz, H., Toenjes, R., Kratz, K.-L., Pfeiffer, B., Beers, T.C., Cowan, J. J., & Hill, V. 2002, ApJ, submitted
Sneden, C., Cowan, J. J., Ivans, I. I., Fuller, G. M., Burles, S., Beers, T. C., Lawler, J. E. 2000, ApJ, 533, L139
Sneden, C., Cowan, J. J., Lawler, J. E., Burles, S., Beers, T. C., & Fuller, G. M. 2002, ApJ, 566, L25
Sneden, C., McWilliam, A., Preston, G. W., Cowan, J. J., Burris, D. L., & Armosky, B. J. 1996, ApJ, 467, 819
Takahashi, K., Witti, J., & Janka, H.-Th. 1994, A&A, 286, 857
Terasawa, M., Sumiyoshi, K., Kajino, T., Mathews, G. J., & Tanihata, I. 2001, ApJ, 562, 470

Thompson, T. A., Burrows, A., & Meyer, B. S. 2001, ApJ, 562, 887
Tsujimoto, T., Shigeyama, T., & Yoshii, Y. 2000, ApJ, 531, L33
Utsunomiya, H., Yonezawa, Y., Akimune, H., Yamagata, T., Ohta, M., Fujishiro, M., Toyokawa, H., & Phgaki, H. 2001, Phys. Rev. C, 63, 18801
Wanajo, S., Kajino, T., Mathews, G. J., & Otsuki, K. 2001, ApJ, 554, 578
Woosley, S. E., Wilson, J. R., Mathews, G. J., Hoffman, R. D., & Meyer, B. S. 1994, ApJ, 433, 229